

Surface Plasmon Instability Leading to Emission of Radiation

Godfrey Gumbs^{1,2}, Andrii Iurov¹, Danhong Huang³, and Wei Pan⁴

¹*Department of Physics and Astronomy, Hunter College of the City University of New York, 695 Park Avenue, New York, NY 10065, USA*

²*Donostia International Physics Center (DIPC),*

P de Manuel Lardizabal, 4, 20018 San Sebastian, Basque Country, Spain

³*Air Force Research Laboratory, Space Vehicles Directorate, Kirtland Air Force Base, NM 87117, USA*

⁴*Sandia National Laboratory, Albuquerque, NM 87185, USA*

We propose a new energy conversion approach from a dc electric field to a terahertz wave based on hybrid semiconductors by combining two-dimensional (2D) crystalline layers and a thick conducting material with possible applications as a source of coherent radiation. The hybrid nano-structure may consist of a single or pair of sheets of graphene, silicene or a 2D electron gas as would occur at a semiconductor hetero-interface. When an electric current is passed through a layer, we discover that the low-frequency plasmons may become unstable beyond a critical wave vector q_c . However, there is no instability for a single driven layer far from the conductor and the instability of an isolated pair of 2D layers occurs only at ultra long wavelengths. To bring in frequency agility for this spontaneous radiation, we manipulate the surface-plasmon induced instability, which leads to the emission of radiation (spiler), to occur at shorter wavelengths by choosing the conductor electron density, layer separation, distances of layers from the conductor surface and the driving-current strength. Applications of terahertz radiation from spiler for chemical analysis, security scanning, medical imaging and telecommunications are expected.

PACS numbers: 73.21.-b, 71.70.Ej, 73.20.Mf, 71.45.Gm, 71.10.Ca, 81.05.ue

Possible sources of terahertz (THz) radiation have been investigated for several years now. These frequencies cover the electromagnetic (EM) spectrum lying between microwave and far-infrared. By epitaxially growing layers of different semiconductors (including GaAs, GaAs/AlGaAs, InAs/InGaAs), multiple quantum-well layers, which emit high-power THz radiation across a wide frequency range, have been fabricated. The work reported so far covers ultra-long wavelength emission, phase/mode-locking, multiple color generation, photonic crystal structures, and improved laser performance with respect to both maximum operating temperature and peak output power. It was predicted by Kempa, et al. [1] (see also Ref. [2]) that when a current is passed through a stationary electron gas, the Doppler shift in response frequency of this two-component plasma leads to a spontaneous generation of plasmon excitations at ultra-long wavelengths and subsequent Cherenkov radiation [3] at sufficiently high carrier drift velocities. For their model, the process is irreversible based on the lack of time reversal symmetry (Onsager's principle of microscopic reversibility) [4]. Similar conclusions are expected for monolayer graphene which is characterized by massless Dirac fermions where the energy dispersion is linear in the wave vector \mathbf{k}_{\parallel} or a nanosheet of silicene consisting of silicon atoms, which has been synthesized [5]. In the same group of the periodic table with graphene, silicene is predicted to exhibit similar electronic properties. Additionally, it has the advantage over graphene in its compatibility with Si-based device technologies.

The role played by plasma excitations in the THz response of low-dimensional microstructures has received considerable attention [6–15]. Plasmon modes of quantum-well transistor structures with frequencies in the THz range may be excited with the use of far-infrared (FIR) radiation and other means [16]. A split grating gate design has been found to significantly enhance FIR response [17–20]. Under this scheme, however, the stimulated EM radiation require either a population inversion [21] or a quantum coherence [22], or a condensation [23]. The EM radiation can also be generated by transferring energy from optical field to another [24].

Here, we explore a new energy conversion approach, i.e., from an applied dc electric field to an optical field based on a current-driven induced instability. The primary objective of the Letter is to expand the materials platform by exploiting the functionality of a composite nano-system consisting of a thick conductor (including a heavily-doped semiconductor) which is Coulomb coupled to 2D layered materials. The Coulomb coupling of the plasmons in a layer to the surface plasmon on the conductor results in a surface-plasmon instability that leads to the emission of radiation (spiler). The predicted tunable spiler radiation relies on a current-induced plasmon instability and comes after the plasmon grows in the time domain at a rate which is determined by the surface-plasmon frequency, the 2D layer separation, the distance of the 2D layers from the conducting surface and the driving-current strength.

In our formalism, we consider a nano-scale system consisting of a pair of 2D layers and a thick conducting material. The layer may be monolayer graphene or a 2DEG such as a semiconductor inversion layer or high electron mobility

transistor. The graphene layer may have a gap, thereby extending the flexibility of the composite system that also incorporates a thick conducting layer.

In our notation, the structure has a double layer located at $z = a_1$ and $z = a_2$ ($0 < a_1 < a_2$) interacting with each other as well as the semi-infinite system with its surface lying in the xy -plane at $z = 0$. The longitudinal excitation spectra of allowable modes will be determined from a knowledge of the frequency-dependent non-local dielectric function $\epsilon(\mathbf{r}, \mathbf{r}'; \omega)$ which depends on the position coordinates \mathbf{r}, \mathbf{r}' and frequency ω . Alternatively, the normal modes correspond to the resonances of the inverse dielectric function $K(\mathbf{r}, \mathbf{r}'; \omega)$, satisfying $\int d\mathbf{r}' K(\mathbf{r}, \mathbf{r}'; \omega) \epsilon(\mathbf{r}', \mathbf{r}''; \omega) = \delta(\mathbf{r} - \mathbf{r}'')$. The significance of $K(\mathbf{r}, \mathbf{r}'; \omega)$ is that it embodies many-body effects [25] through screening by the medium of an external potential $U(\mathbf{r}'; \omega)$ to produce an effective potential $V(\mathbf{r}; \omega) = \int d\mathbf{r}' K(\mathbf{r}, \mathbf{r}'; \omega) U(\mathbf{r}'; \omega)$. The self-consistent field equation for $K(\mathbf{r}, \mathbf{r}'; \omega)$ is in integral form, after Fourier transforming parallel to the xy -plane and suppressing the in-plane wave number q_{\parallel} and frequency ω , leading to

$$K(z_1, z_2) = K_{SI}(z_1, z_2) - \sum_{j=1}^2 \int_{-\infty}^{\infty} dz' \int_{-\infty}^{\infty} dz'' K_{SI}(z_1, z') \alpha_{2D;j}(z', z'') K(z'', z_2). \quad (1)$$

Here, the polarization function for the 2D structure is given by

$$\alpha_{2D;j}(z', z'') = \int_{-\infty}^{\infty} dz''' v(z' - z''') D_j(z''', z''), \quad (2)$$

where $v(z - z') = (2\pi e^2 / \epsilon_s q_{\parallel}) \exp(-q_{\parallel} |z - z'|)$, $\epsilon_s = 4\pi\epsilon_0\epsilon_r$, and the 2D response function obeys $D_j(z''', z'') = \Pi_{2D;j}^{(0)}(q_{\parallel}, \omega) \delta(z''' - a_j) \delta(z'' - a)$ with $\Pi_{2D;j}^{(0)}(q_{\parallel}, \omega)$ as the single-particle in-plane response. Upon substituting this form of the polarization function for the monolayer into Eq. (1), we have

$$K(z_1, z_2) = K_{SI}(z_1, z_2) - \sum_{j=1}^2 \Pi_{2D;j}^{(0)}(q_{\parallel}, \omega) \int_{-\infty}^{\infty} dz' K_{SI}(z_1, z') v(z' - a_j) K(a_j, z_2). \quad (3)$$

We now set $z_1 = a_1$ and $z_1 = a_2$ in turn in Eq. (3) and solve simultaneously the pair of equations for $K(a_1, z_2)$ and $K(a_2, z_2)$ to obtain

$$\begin{bmatrix} K(a_1, z_2) \\ K(a_2, z_2) \end{bmatrix} = \frac{1}{S_c^{(2)}(q_{\parallel}, \omega)} \overleftrightarrow{\mathcal{M}}(q_{\parallel}, \omega) \begin{bmatrix} K_{SI}(a_1, z_2) \\ K_{SI}(a_2, z_2) \end{bmatrix}, \quad (4)$$

where $S_c^{(2)}(q_{\parallel}, \omega) = \text{Det}[\overleftrightarrow{\mathcal{M}}(q_{\parallel}, \omega)]$ with the coefficient matrix given by

$$\overleftrightarrow{\mathcal{M}}(q_{\parallel}, \omega) = \begin{bmatrix} 1 + \Pi_{2D;2}^{(0)}(q_{\parallel}, \omega) \int_{-\infty}^{\infty} dz' K_{SI}(a_2, z') v(z' - a_2) & -\Pi_{2D;2}^{(0)}(q_{\parallel}, \omega) \int_{-\infty}^{\infty} dz' K_{SI}(a_1, z') v(z' - a_2) \\ -\Pi_{2D;1}^{(0)}(q_{\parallel}, \omega) \int_{-\infty}^{\infty} dz' K_{SI}(a_2, z') v(z' - a_1) & 1 + \Pi_{2D;1}^{(0)}(q_{\parallel}, \omega) \int_{-\infty}^{\infty} dz' K_{SI}(a_1, z') v(z' - a_1) \end{bmatrix}. \quad (5)$$

In our numerical calculations, we shall use $K_{SI}(z, z')$ given in Eq.(30) of Ref.[26]. Substituting the results for $K_{SI}(a_1, z_2)$ and $K_{SI}(a_2, z_2)$ into Eq. (4), we obtain the complete inverse dielectric function for a pair of 2D conducting planes interacting with each other and a semi-infinite conducting material. The plasmon excitation frequencies are determined by the zeros of $S_c^{(2)}(q_{\parallel}, \omega)$. Furthermore, the effect of the inverse dielectric function for the semi-infinite structure $K_{SI}(z, z'; q_{\parallel}, \omega)$ leads to coupling between the two layers and of each layer with the bulk and surface of the neighboring material. As a matter of fact, our result for the plasmon dispersion relation generalizes that obtained by Das Sarma and Madhukar [27–29] for a biplane. We obtain in the local limit [26]

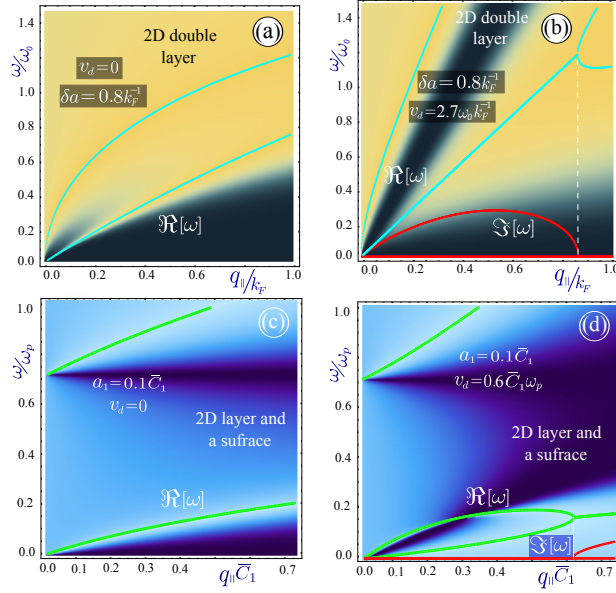


FIG. 1: (Color online) Complex frequencies yielding the plasmon dispersion (real part $\Re[\omega]$) and inverse growth rate (imaginary part $\Im[\omega]$) for a pair of free-standing 2D layers with separation δa [panels (a) and (b)] and for the case of one layer Coulomb coupled to a semi-infinite conducting substrate [panels (c) and (d)]. The frequency unit in (a) and (b) is $\omega_0 = \sqrt{2\pi e^2 C_1 k_F / \epsilon_s}$, while the wave vector q_{\parallel} is measured in units of the Fermi wave vector k_F . In the case of two layers, the instability domain ranges from the origin to a certain value of q_{\parallel} at the bifurcation point, i.e., the ultra-long wavelength region. The position of this bifurcation point depends on δa and the drift velocity v_d . The instability domain changes drastically in the presence of a surface, as demonstrated in the two lower panels (c) and (d) with q_c shifted from zero to shorter wavelengths. Here, the current is passed through the 2D layer in panel (d), and it is passed through the bottom 2D layer in panel (b). The carrier density, temperatures or doping densities are chosen such that $\bar{C}_2 = 1.2\bar{C}_1$ for all cases.

$$\begin{aligned}
S_c^{(2)}(q_{\parallel}, \omega) &= \left\{ 1 + \frac{2\pi e^2}{\epsilon_s q_{\parallel}} \Pi_{2D;2}^{(0)}(q_{\parallel}, \omega) \left[1 + e^{-2q_{\parallel} a_2} \frac{\omega_p^2}{2\omega^2 - \omega_p^2} \right] \right\} \\
&\times \left\{ 1 + \frac{2\pi e^2}{\epsilon_s q_{\parallel}} \Pi_{2D;1}^{(0)}(q_{\parallel}, \omega) \left[1 + e^{-2q_{\parallel} a_1} \frac{\omega_p^2}{2\omega^2 - \omega_p^2} \right] \right\} \\
&- \left(\frac{2\pi e^2}{\epsilon_s q_{\parallel}} \right)^2 \Pi_{2D;1}^{(0)}(q_{\parallel}, \omega) \Pi_{2D;2}^{(0)}(q_{\parallel}, \omega) \left[e^{-q_{\parallel} |a_1 - a_2|} + e^{-q_{\parallel} (a_1 + a_2)} \frac{\omega_p^2}{2\omega^2 - \omega_p^2} \right]^2. \quad (6)
\end{aligned}$$

Setting $a_1 = a$ and letting $a_2 \rightarrow \infty$ in Eq. (5), the off-diagonal matrix elements tend to zero and the element in the first row and first column reduces to unity. Subsequently, the dispersion equation for a single layer interacting with the substrate is given by the zeros of the matrix element in the second row and second column. Using the long-wavelength limit ($q \ll k_F$), we find $\Pi_{2D;j}^{(0)}(q_{\parallel}, \omega) \approx -C_j q_{\parallel}^2 / \omega^2$. For a 2DEG, we have $C = n_{2D} / m_{2D}^*$; for doped graphene, we have $C = (2\mu / \pi \hbar^2) [1 - (\Delta^2 / \mu^2)]$, where μ is the chemical potential and Δ is the gap between valence and conduction bands; for intrinsic graphene whose plasmon excitations are induced by temperature, $C = (2 \ln 2) k_B T / \pi \hbar^2$ [30]. Consequently, we find the plasmon frequency as follows [31]: $\omega^2 = K_1 \pm \sqrt{K_2}$ with K_1 and K_2 defined by $K_1 = \bar{C} q_{\parallel} \omega_p^2 / 2 + (\omega_p / 2)^2$ and $K_2 = \bar{C} q_{\parallel} \omega_p^4 \exp(-2q_{\parallel} a) / 2 + (\omega_p / 2)^4 (1 - 2\bar{C} q_{\parallel})^2$, where $\bar{C} = 2\pi e^2 C / (\epsilon_s \omega_p^2)$. Additionally, within this long-wavelength limit, these expressions yield the plasmon excitation frequencies $\omega_1 / \omega_p \simeq q_{\parallel} \sqrt{2\bar{C} a}$ and $\omega_2 / \omega_p \simeq 1 / \sqrt{2} + \bar{C} q_{\parallel} / \sqrt{2}$ which are both linear in q_{\parallel} and unlike the $\sqrt{q_{\parallel}}$ -dependence for free-standing graphene or the 2DEG [32–37].

In Ref. [38], it was demonstrated that the plasmon excitations in graphene has a linear dispersion rather than a square root dependence on the wave vector. This startling result came as a surprise because theoretical calculations on free-standing graphene clearly do not predict a linear dependence in the long-wavelength limit. As a matter of

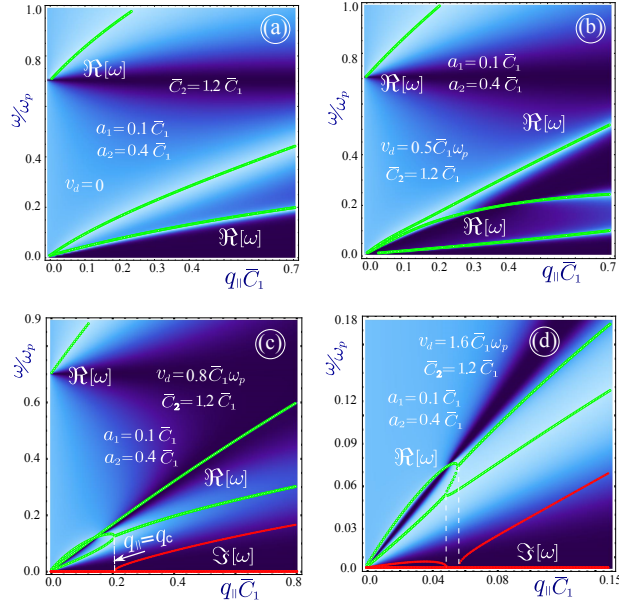


FIG. 2: (Color online) Plasmon dispersion relation and inverse growth rate for a pair of 2D layers and a semi-infinite conducting medium. The plasma frequency for the semi-infinite medium is ω_p . The layers are located at $a_1 = 0.1\bar{C}_1$ and $a_2 = 0.4\bar{C}_1$ with respect to the surface. Each panel corresponds to a different drift velocity with $v_d/\omega_p = 0, 0.5\bar{C}_1, 0.8\bar{C}_1$ and $1.6\bar{C}_1$. Here, the current is passed through the bottom 2D layer. Panel (a) with $v_d = 0$ corresponds to the solutions in Eq. (7). Panel (b) shows that for a small v_d an additional plasmon branch appears, but all solutions are stable. The carrier concentrations, chemical potentials or temperatures in the layers are such that $\bar{C}_2 = 1.2\bar{C}_1$ for all cases. Either of the two lowest plasmon branches might become unstable, depending on v_d . The Rabi-type splitting of the plasmon excitation branches by the external electric field is attributed to quasiparticles with different excitation energies for the same wavelength. After the Rabi “loop” closes at q_c in (c), the lowest branch becomes unstable with finite imaginary part illustrated by the red curve. In (d), the lowest plasmon branch has an instability for two separate ranges of wave vector.

fact, this linear dependence of plasmon frequency on wave vector was attributed to local field corrections to the random-phase approximation. In our notation, $\bar{C}_j = 2\pi e^2 C_j / (\epsilon_s \omega_p^2)$ for $j = 1, 2$. The spectral function yields real frequencies. A plane interacting with the half-space has two resonant modes. Each pair of 2D layers interacting in isolation far from the semi-space medium supports a symmetric and an antisymmetric mode [27]. In the absence of a driving current, the analytic solutions for the plasmon modes of a pair of 2D layers that are Coulomb coupled to a half-space are given by

$$\begin{aligned}
 \frac{\Omega_1(q_{\parallel})}{\omega_p} &= 1/\sqrt{2} + q_{\parallel}(\bar{C}_1 + \bar{C}_2)/\sqrt{2} + \mathcal{O}[q_{\parallel}^2], \\
 \frac{\Omega_2(q_{\parallel})}{\omega_p} &= q_{\parallel} \sqrt{\bar{C}_1 a_1 + \bar{C}_2 a_2 + \sqrt{\mathcal{A}}} + \mathcal{O}[q_{\parallel}^2], \\
 \frac{\Omega_3(q_{\parallel})}{\omega_p} &= q_{\parallel} \sqrt{\bar{C}_1 a_1 + \bar{C}_2 a_2 - \sqrt{\mathcal{A}}} + \mathcal{O}[q_{\parallel}^2],
 \end{aligned} \tag{7}$$

where $\mathcal{A} \equiv (\bar{C}_1 a_1 - \bar{C}_2 a_2)^2 + 4\bar{C}_1 \bar{C}_2 a_1^2$ and the term $4\bar{C}_1 \bar{C}_2 a_1^2$ plays the role of “Rabi coupling”. Clearly, for long wavelengths, only $\Omega_1(q_{\parallel})$ depends on ω_p . However, the excitation spectrum changes dramatically when a current is driven through the configuration. Under a constant electric field, the carrier distribution is modified, as may be obtained by employing the relaxation-time approximation in the equation of motion for the center-of-mass momentum. For a parabolic energy band for carriers with effective mass m^* and drift velocity \mathbf{v}_d determined by the electron mobility and the external electric field, the electrons in the medium are redistributed. This is determined by a momentum shift in the wave vector $\mathbf{k}_{\parallel} \rightarrow \mathbf{k}_{\parallel} - m^* \mathbf{v}_d / \hbar$ in the thermal-equilibrium energy distribution function $f_0(\epsilon_{\mathbf{k}})$. By making a change of variables in the well-known Lindhard polarization function $\Pi^{(0)}(q, \omega)$, this effect is equivalent to a frequency shift $\omega \rightarrow \omega - \mathbf{q} \cdot \mathbf{v}_d$. For massless Dirac fermions in graphene with linear energy dispersion, this Doppler shift in frequency is not in general valid for arbitrary wave vector. This is our conclusion after we relate the surface current

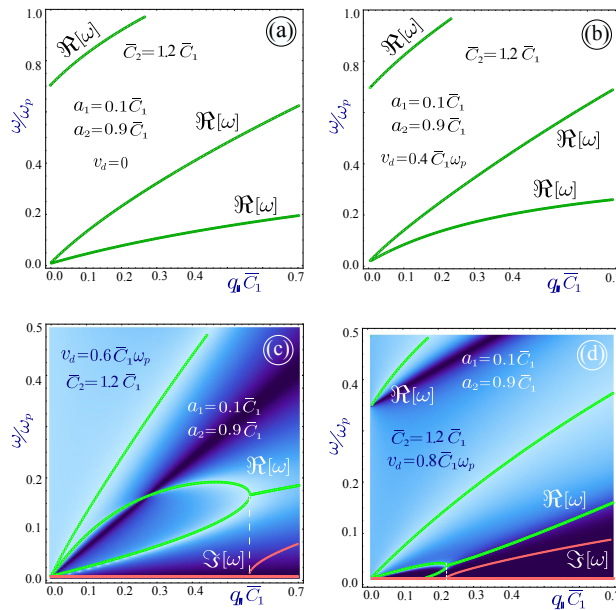


FIG. 3: (Color online) Plasmon dispersion relation and inverse growth rate for a pair of 2D layers and a semi-infinite conducting medium. The layers are located at $a_1 = 0.1\bar{C}_1$ and $a_2 = 0.9\bar{C}_1$ with respect to the surface. Each panel is attributed to a different drift velocity with $v_d/\omega_p = 0, 0.4\bar{C}_1, 0.6\bar{C}_1$ and $0.8\bar{C}_1$. In panels (a), (b) and (c), the current is passed through the bottom 2D layer but in panel (d), the current is passed through the semi-infinite medium. The particle concentrations, temperatures or chemical potentials for the 2D layers is such that $\bar{C}_2 = 1.2\bar{C}_1$ for all cases. Only the lowest plasmon branch becomes unstable beyond a critical wave vector q_c . The Rabi-type splitting of the plasmon excitation branches by the external electric field indicates the excitation of two quasiparticles with different excitation energies at the same wavelength.

density to the center-of-mass wave vector in a steady state. Our calculation shows that the redistribution of electrons leads to a shift in the wave vector appearing in the Fermi function by the center-of-mass wave vector $\mathbf{K}_0 = (k_F/v_F)\mathbf{v}_d$, where k_F and v_F are the Fermi wave vector and velocity, respectively. However, in the long-wavelength limit, $q_{\parallel} \rightarrow 0$, the Doppler shift in frequency is approximately obeyed. Consequently, regardless of the nature of the 2D layer represented in the dispersion equation we may replace $\omega \rightarrow \omega - \mathbf{q} \cdot \mathbf{v}_d$ in the dispersion equation in the presence of an applied electric field at long wavelengths.

To highlight the effect due to a surface in spiler, as a comparison we first present in Figs. 1(a) and 1(b) the plasmon dispersion for an isolated pair of 2D layers in the absence [27] and presence [1] of a current, respectively. When a substrate surface plasmon is not contributing, the plasmon instability starts at $q_{\parallel} = 0$ and exists over a finite range until a bifurcation point is reached for q_{\parallel} . By going beyond this bifurcation point, the interlayer Coulomb coupling is effectively suppressed, leading to one uncoupled 2D-sheet plasma and two current-split 2D-sheet plasmon modes. However, when a surface plasmon interacts with the two 2D layers, the plasmon instability may be moved to shorter wavelengths, as we clearly illustrated in Figs. 1(d), where we show the results when spiler consists of a 2D layer and a semi-infinite conducting medium. Plasmon remains stable in a single current-driven 2D layer. In the presence of the surface plasmon, as $v_d/\omega_p = 0.6\bar{C}_1$ in (d) the plasmon instability occurs outside the closed Rabi “loop”, i.e., $q_{\parallel} > q_c$ (q_c is the critical wave vector), and at shorter wavelengths by pushing q_c significantly above zero.

In order to get a full understanding of the mechanism for instability shown in Fig. 1, in Fig. 2 we have numerically investigated the effect of a passing current through a layer of 2DEG, graphene or silicene which is Coulomb coupled to a conductor. Specifically, we consider a pair of 2D layers and a semi-infinite medium such as a heavily-doped semiconductor. We present in Fig. 2 both the plasmon dispersion and the inverse growth rate. Each panel shows results for a different drift velocity given by $v_d/\omega_p = 0, 0.5\bar{C}_1, 0.8\bar{C}_1$ and $1.6\bar{C}_1$. In the absence of a current, panel (a) shows that there are three plasmon excitation branches, which are stable as given by Eq. (7). At low v_d , panel (b) demonstrates that the plasmons are still stable. However, as v_d is increased further, the lowest branches may become unstable as in (c) and (d) through the appearance of a positive imaginary part for the frequency. There is a threshold value for v_d beyond which the plasmon excitation becomes unstable. On the other hand, the existence of the surface plasmon greatly screens both the interlayer and intralayer Coulomb couplings as $q_{\parallel} a_1 \ll 1$ in the range of $\omega/\omega_p \ll 1$. This stabilizes the plasmon excitation for $q_{\parallel} < q_c$ by suppressing the interlayer coupling as shown in

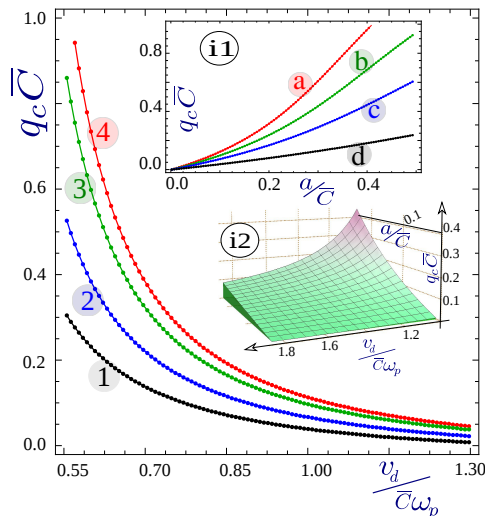


FIG. 4: (Color online) Plot of the the critical wave vector where the plasmon instability occurs for a single 2D layer Coulomb coupled to a thick conducting medium as a function of the drift velocity v_d . The curves 1-4 correspond to chosen separations from the surface with $a/\bar{C} = 1.1, 1.0, 0.8$ and 0.6 . Inset *i1* shows the variation of q_c with a . Curves *a-d* correspond to $v_d = 1.0, 1.10, 1.25$ and 1.7 in units of $\bar{C}\omega_p$. Inset *i2* is a 3D plot of q_c as functions of both a and v_d .

(c). As v_d increases to $1.6\bar{C}_1\omega_p$ in (d), q_c reduces almost to zero, but the wide stable region in (c) is squeezed into a narrow belt. The occurrence of such a new unstable region starting from $q_{\parallel} = 0$ is a combined result from both the surface-induced softening of the two 2D-sheet plasma modes to two acoustic-like plasmon modes as well as the strong interlayer coupling for small layer separation. To some extent, this feature is similar to the result displayed in Fig. 1(b) for the isolated pair of 2D layers.

Figure 3 illustrates our results for larger 2D layer separations from each other compared to the case in Fig. 2. Panel (a) again corresponds to the analytic solutions in Eq. (7) when $v_d = 0$. The plasmon excitations are all still stable in (b) at $v_d/\omega_p = 0.4\bar{C}_1$. However, as v_d is increased further in (c) and (d), an instability appears at q_c , which is exactly where the Rabi “loop” for plasmon excitations closes in the two lower panels. Beyond q_c , the plasmon becomes unstable corresponding to opposite phase velocities for two current-split plasmon branches. The loop shape is quite different for current passing through the 2D layer [in (c)] and the semi-infinite medium [in (d)]. We also note that by adjusting the layer separation, we may change q_c value for controlling the onset of the plasmon instability. With such a large interlayer separation, the interlayer interaction becomes very weak and the system effectively behaves like the single current-driven 2D layer coupled to a conducting surface, similar to that in Figs. 1(d).

Physically, from the point of view of momentum space, electrons may only occupy momentum space within the range of $|\mathbf{k}_{\parallel}| \leq k_F$ at zero temperature in a state of thermal equilibrium, where k_F is the electron Fermi wave number and $\varepsilon(k_F) = \varepsilon(-k_F) = E_F$ is the Fermi energy. When a current is passed through the electron gas, electrons are driven out from this thermal-equilibrium state and their population becomes asymmetrical with respect to $k_{\parallel} = 0$. In this case, the Fermi energy E_F is split into $E_{F,+} = \varepsilon(k_F + K_0)$ and $E_{F,-} = \varepsilon(-k_F + K_0)$ with $E_{F,+} > E_{F,-}$, where $\hbar K_0$ represents the electron center-of-mass momentum. In this shifted Fermi-Dirac distribution model, electrons in such a non-equilibrium state are energetically unstable, and the higher-energy electrons in the range $k_F \leq k \leq k_F + K_0$ tend to decay into lower-energy empty states by emitting EM waves and phonons to ensure the conservations of total momentum and energy.

The current-driven asymmetric electron distribution in \mathbf{k}_{\parallel} space leads to an induced oscillating polarization current or a “dipole radiator”. If two electron gas layers are placed close enough, the in-phase interlayer Coulomb interaction will give rise to a dipole-like plasmon excitation, similar to that of a single layer. On the other hand, the out-of-phase interlayer Coulomb coupling will lead to a quadruple-like excitation. This quadruple-like plasmon excitation can be effectively converted into a transverse EM field in free space if a surface grating is employed.

The surface-induced instability in spiler may lead to EM radiation, and the lower edge of its radiation frequency can be tuned directly by q_c to cover the THz frequency range. Here, we present in Fig. 4 the dependence of controlling parameter q_c as functions of v_d and separation a for a single 2D layer coupled to surface plasmon, where q_c is increased

with either reducing v_d or increasing a . These results clearly demonstrate significant shifts of q_c within the desired ranges for operations of both photodetectors and EM-wave devices.

In summary, we are proposing a spiler quantum plasmonic device which employs 2D layers such as graphene/III-V semiconductor hybrids in combination with a thick conducting material with clean interfaces. We find that the spiler spontaneously emits EM radiation when a current is passed through the 2D layer or the underlying conductor to make the plasmons become unstable at a specific frequency and wave number. It is possible to tune the onset of plasmon instability by selecting the properties of the nanosheet or frequency of the surface plasmon, i.e., the substrate. The surface plasmon plays a crucial role in giving rise to the splitting and the concomitant streams of quasiparticles whose phase velocities are in opposite directions when the instability takes place. The emitted EM radiation may be coupled easily outward to a free space by a grating on the surface. Finally, we note that in presenting our numerical results, we measured frequency in terms of the bulk plasmon frequency which, typically for conductors, is $\hbar\omega_p \sim 0.5\text{ eV}$. Either for intrinsic graphene, doped monolayer graphene or an inversion layer 2DEG, we have $\bar{C} \sim 10^{-7}\text{ m}$ and $v_d \sim 10^6\text{ m/s}$. The frequency unit used in Fig. 1 is $\omega_0 = \sqrt{2\pi e^2 C_1 k_F / \epsilon_s}$ which is of the same order as ω_p .

Experimentally, the emitted EM radiation of a spiler device can be detected by heterodyne mixing technique using a planar Schottky diode [39]. In this experiment, the mixing of the EM radiation against a molecular laser line is known to give a high precision measurement of the EM radiation frequency and can also show transient turn-on behavior in a pulsed spiler device.

The spontaneous EM radiation from the proposed spiler does not require a population inversion in a laser, a coupling-field quantum coherence in amplification without inversion and a exciton-polariton condensation [21–23]. Instead, it depends on energy conversion [24] from an applied dc electric field to an optical field based on a current-induced plasmon instability. The radiation frequency of the spiler is tunable and covers the whole THz range. Terahertz waves are able to penetrate materials that block visible light and have a wide range of possible applications, including chemical analysis, security scanning, medical imaging, and telecommunications.

This research was supported by contract # FA 9453-13-1-0291 of AFRL. DH would like to thank the Air Force Office of Scientific Research (AFOSR) for its support. We thank Oleksiy Roslyak and Antonios Balassis for helpful discussions. WP was supported by the U.S. Department of Energy, Office of Science, Basic Energy Sciences, Materials Sciences and Engineering Division.

-
- [1] K. Kempa, P. Bakshi, J. Cen, and H. Xie, Phys. Rev. B **43**, 9273 (1991).
 - [2] S. Tariq, A. M. Mirza, and W. Masood, Phys. Plasmas **17**, 102705 (2010).
 - [3] M. Akbari-Moghanjoughi, Phys. Plasmas **21**, 053301 (2014).
 - [4] L. Onsager, Phys. Rev. **37**, 405 (1931).
 - [5] C.-C. Liu, W. Feng, and Y. Yao, Phys. Rev. Lett. **107**, 076802 (2011).
 - [6] S. J. Allen, D. S. Tsui, and R. A. Logan, Phys. Rev. Lett. **38**, 980 (1977).
 - [7] D. S. Tsui, S. J. Allen, R. A. Logan, A. Kamgar, and S. N. Coopersmith, Surf. Sci. **73**, 419 (1978).
 - [8] S. Katayama, J. Phys. Soc. Japan **60**, 1123 (1991); Surf. Sci. **263**, 359 (1992).
 - [9] C. Steinebach, D. Heitmann, and V. Gudmundsson, Phys. Rev. B **56**, 6742 (1997).
 - [10] B. P. van Zyl and E. Zaremba, Phys. Rev. B **59**, 2079 (1999).
 - [11] S. A. Mikhailov, Phys. Rev. B **58**, 1517 (1998).
 - [12] O. R. Matov, O. F. Meshkov, and V. V. Popov, JETP **86**, 538 (1998).
 - [13] O. R. Matov, O. V. Polischuk, and V. V. Popov, JETP **95**, 505 (2002).
 - [14] G. Gumbs and D. H. Huang, Phys. Rev. B **75**, 115314 (2007).
 - [15] D. H. Huang, G. Gumbs, P. M. Alsing, and D. A. Cardimona, Phys. Rev. B **77**, 165404 (2008).
 - [16] N. J. M. Horing, H. C. Tso, and G. Gumbs, Phys. Rev. B **36**, 1588 (1987).
 - [17] E. A. Shaner, A. D. Grine, M. C. Wanke, Mark Lee, J. L. Reno, and S. J. Allen, IEEE Photon. Technol. Lett. **18**, 1925 (2006).
 - [18] V. V. Popov, T. V. Teperik, G. M. Tsymbalov, X. G. Peralta, S. J. Allen, N. J. M. Horing, and M. C. Wanke, Semicond. Sci. Technol. **19**, S71 (2004).
 - [19] A. Balassis and G. Gumbs, J. Appl. Phys. **106**, 103102 (2009).
 - [20] A. Balassis, G. Gumbs, and D. H. Huang, Proc. SPIE **7467**, 74670O (2009).
 - [21] A. L. Schawlow and C. H. Townes, Phys. Rev. **112**, 1940 (1958).
 - [22] H. Fearn, C. Keitel, M. O. Scully, and S. Y. Zhu, Opt. Commun. **87**, 323 (1992).
 - [23] S. Christopoulos, G. B. H. von Högersthal, A. J. D. Grundy, P. G. Lagoudakis, A.V. Kavokin, J. J. Baumberg, G. Christmann, R. Butté, E. Feltn, J.-F. Carlin, and N. Grandjean, Phys. Rev. Lett. **98**, 126405 (2007).
 - [24] D. J. Bergman and M. I. Stockman, Phys. Rev. Lett. **90**, 027402 (2003).

- [25] K. A. Kouzakov and J. Berakdar, Phys. Rev. A **85**, 022901 (2012).
- [26] N. J. M. Horing, E. Kamen, and H.-L. Cui, Phys. Rev. B **32**, 2184 (1985).
- [27] S. Das Sarma and A. Madhukar, Phys. Rev. B **23**, 805 (1981).
- [28] K. Pohl, B. Diaconescu, G. Vercelli, L. Vattuone, V. M. Silkin, E. V. Chulkov, P. M. Echenique, and M. Rocca, Europhys. Lett. **90**, 57006 (2010).
- [29] R. E. V. Profumo, R. Asgari, M. Polini, and A. H. MacDonald, Phys. Rev. B **85** 085443 (2012).
- [30] S. Das Sarma and Q. Li, Phys. Rev. B **87**, 235418 (2014).
- [31] N. J. M. Horing, Phys. Rev. B **80**, 193401 (2009).
- [32] B. Wunsch, T. Stauber, F. Sols, and F. Guinea, New J. Phys. **8**, 318 (2006).
- [33] P. K. Pyatkovskiy, J. Phys.: Condens. Matt. **21**, 025506 (2009).
- [34] K. W.-K. Shung, Phys. Rev. B **34**, 979 (1986).
- [35] K. W.-K. Shung, Phys. Rev. B **34**, 1264 (1986).
- [36] T. Ando, J. Phys. Soc. Jpn. **75**, 074716 (2006).
- [37] E. H. Hwang and S. Das Sarma, Phys. Rev. B **75**, 205418 (2007).
- [38] C. Kramberger, R. Hambach, C. Giorgetti, M. H. Rummeli, M. Knupfer, J. Fink, B. Büchner, L. Reining, E. Einarsson, S. Maruyama, F. Sottile, K. Hannewald, V. Olevano, A. G. Marinopoulos, and T. Pichler, Phys. Rev. Lett. **100**, 196803 (2008).
- [39] M. Lee, M. C. Wanke, M. Lerttamrab, E. W. Young, A. D. Grine, J. L. Reno, P. H. Siegel, and R. J. Dengler, IEEE J. Selected Topics Quantum Electr. **14**, 370 (2008).